Springer

Available online at https://link.springer.com
http://www.jhydrod.com/
2018,30(1):62-69
https://doi.org/10.1007/s42241-018-0006-9

SPH modeling of fluid-structure interaction*

Luhui Han, Xiangyu Hu
Department of Mechanical Engineering, Technical University of Munich, Garching85747, Germany

(Received October 22, 2017, Accepted December 7, 2017)

Abstract: This work concerns numerical modeling of fluid-structure interaction (FSI) problems in a uniform smoothed particle hydrodynamics (SPH) framework. It combines a transport-velocity SPH scheme, advancing fluid motions, with a total Lagrangian SPH formulation dealing with the structure deformations. Since both fluid and solid governing equations are solved in SPH framework, while coupling becomes straightforward, the momentum conservation of the FSI system is satisfied strictly. A well-known FSI benchmark test case has been performed to validate the modeling and to demonstrate its potential.

Key words: Fluid-structure interaction (FSI), smoothed particle hydrodynamics (SPH), total Lagrangian formulation

Introduction

Fluid-structure interaction (FSI) can be found in many natural phenomena, such as birds flying and fish swimming. Meanwhile, it also plays a very important role in the design of many engineering systems, e.g., aircrafts, engines and bridges. Although the mechanical behaviors of the FSI systems are quite different, their common essentials are interactions between movable or deformable structures and internal or external fluid flows[1].

Since FSI problems usually involve nonlinear fluid and solid dynamics, which are too complex to be solved analytically, they mostly have to be analyzed by means of experiments or numerical simulations, and the individual maturity of computational fluid dynamics (CFD) and computational solid dynamics (CSD) in past decades enables it[2]. Accordingly, a number of individual CFD or CSD approaches have already been developed, such as the space-time finite-element method (FEM)[3] and arbitrary Lagrangian Eulerian formulation (ALE)[4]. Because all of these methods are mesh-based, i.e., require that the domain is discretized into individual mesh-elements, they have to take significant efforts on re-meshing to prevent the occurrence of severe mesh distortion[5]. In comparison to conventional mesh-based methods, particle-based meshless methods are intended to approximate the equations of continuum mechanics in the domain only by nodes (particles) without being connected by meshes[6]. Typical meshless methods, which have already been used successfully in solving FSI, are coupled models like smoothed particle hydrodynamics and discrete element method (SPH-DEM)[6] and lattice Boltzmann method-discrete element method (LBM-DEM)[7]. A common advantage of all these meshless methods is that the identification of moving interfaces and deformable boundaries can be handled straightforwardly[8]. Nevertheless, these coupled methods for FSI are still limited for more general applications. They both chose partitioned coupling in the form of "CFD-CSD" by using different discretization schemes to simulate separately the behaviors of fluid and structure, and usually require elaborate consideration for the momentum conservation at fluid-structure interfaces.

SPH method was first developed for simulating astrophysics problems by Lucy[9] and by Gingold and Monaghan[10], and has recently been adapted to many relevant engineering problems, including heat and mass transfer, molecular dynamics, fluid and solid mechanics. Owing to both its significant advantages of handling large deformations in a purely Lagrangian frame in simulation of solid dynamics and its great convenience of capturing breaking, merging, and splashing features in simulation of free surface flows, Antoci et al.[11] successfully proposed an FSI modeling within a uniform SPH framework. Since the same type discretization methods are allowed for a common

***Biography:** Luhui Han (1985-), Male, Ph. D. Candidate,
E-mail: Luhui.han@tum.de
Corresponding author: Xiangyu Hu,
E-mail: Xiangyu.hu@tum.de

description of both the fluid and the solid dynamics in terms of pressure and velocity, both the kinematic and dynamic interface conditions at fluid and solid interfaces became straightforward and easy to be implemented in conservative formulations. Like in Gray et al.'s work[12], the constitutive model, i.e. the linear elastic relation of Hooke's law between stress and deformation tensors, was applied with the incremental Jaumann formulation. As pointed out in Ref. [11], this relation is rate-independent, incrementally linear and reversible. If it is integrated in time with a sufficiently small time step, it can be adopted as a constitutive model when small finite deformations are considered. Other applications by using the same constitutive formulation in solving solid dynamics problems can be found in Refs. [13, 14]. However, observing their simulation results in Refs. [11, 14], one can clearly see that the particle distributions have been shifted after a period of simulation. The initial uniformly distributed particles finally formed into another pattern even in areas without stresses. That is because the conventional SPH method has a shortcoming of inconsistency and the fore-mentioned incremental constitutive model is just an approximation of Hooke's law. To overcome this limit, Vignjevic et al.[15] proposed a total Lagrangian framework for simulating solid dynamics, where Lagrangian kernels were employed directly to solve momentum equation with respect to the reference configuration. Besides, this total Lagrangian formalism takes another advantage of not suffering from tensile instability problems[16].

Inherited from Antoci et al.'s work[11], we proposed a new numerical modeling for FSI problems in this work, where fluid dynamics equations are discretized with conventional Eulerian kernels in current configuration while solid governing equations are solved with Lagrangian kernels in the reference configuration. Finally, a well-known FSI benchmark test case has been performed to validate the current SPH modeling and to demonstrate its potential.

1. Governing equations

1.1 *Fluid equations*

The governing equations for the motion of an isothermal, Newtonian fluid in a Lagrangian frame of current configuration are the continuity equation

$$\frac{\mathrm{d}\rho}{\mathrm{d}t} = -\rho\nabla\cdot\boldsymbol{v} \tag{1}$$

and the momentum-conservation equation

$$\rho\frac{\mathrm{d}\boldsymbol{v}}{\mathrm{d}t} = -\nabla p + \boldsymbol{f}^{(v)} + \rho\boldsymbol{g} \tag{2}$$

with ρ, $\boldsymbol{v}$, t, p, $\boldsymbol{f}^{(v)}$ and $\boldsymbol{g}$ denoting the density of the fluid, the velocity, the time, the pressure, the viscous force and a body-force, respectively.

Based on the weakly compressible SPH approach[11, 17], which is often used to simulate incompressible flows, a linearized equation of state is introduced to estimate the pressure from the density field via

$$p = c_0^2(\rho - \rho_0) \tag{3}$$

where artificial sound speed $c_0 = \sqrt{\varepsilon/\rho_0}$ with ε denoting the compressibility of the fluid. In particular, Monaghan[18] suggests that, in order to limit the admissible density variation to about 1%, the Mach number, i.e., the ratio between the maximal flow speed and c_0, should be about than 0.1.

Assuming incompressibility of the fluid, the viscous force $\boldsymbol{f}^{(v)}$ simplifies to

$$\boldsymbol{f}^{(v)} = \eta\nabla^2\boldsymbol{v} \tag{4}$$

with the dynamic viscosity η.

1.2 *Structure equations*

In this work, the solid model of structure is considered to be elastic and compressible. The governing equations for the motion of a structure have the form ofbalance laws including the balance of mass and momentum.

Following the convention in continuum mechanics, the vector $\boldsymbol{X}$ is used to define the undeformed reference configuration, and vector $\boldsymbol{x}$ defines the deformed current configuration. Assuming the initial state corresponds to the undeformed reference state, the displacement $\boldsymbol{u}$ of a material point, given by the difference between its current position and its original position, can be defined as

$$\boldsymbol{u} = \boldsymbol{x} - \boldsymbol{X} \tag{5}$$

Thus, the deformation gradient $\boldsymbol{F}$, an important variable in the description of body kinematics, can be given by

$$\boldsymbol{F} = \frac{\partial\boldsymbol{x}}{\partial\boldsymbol{X}} = \frac{\partial(\boldsymbol{X}+\boldsymbol{u})}{\partial\boldsymbol{X}} = \mathbf{I} + \frac{\partial\boldsymbol{u}}{\partial\boldsymbol{X}} \tag{6}$$

where $\mathbf{I}$ is a 2nd rank identity matrix.

From a total Lagrangian point of view, the balance of mass adopts the algebraic form given by

$$\rho J - \rho^0 = 0 \tag{7}$$

where ρ^0 is the mass density in the reference configuration, and the Jacobian J is the determinant of $\boldsymbol{F}$. Here we make an important remark that all variables and operators with superscript 0 relate to the reference configuration, i.e., the initial state. Meanwhile, the momentum balance equation is reformed to

$$\rho^0 \frac{\mathrm{d}^2 \boldsymbol{x}}{\mathrm{d}t^2} = \nabla^0 \cdot \boldsymbol{P} + \rho^0 \boldsymbol{g} \tag{8}$$

In the above, ∇^0 is the gradient operator in the reference configuration and $\boldsymbol{P}$ is the 1st Piola-Kirchhoff stress tensor. In contrast to the Cauchy stress tensor $\boldsymbol{\sigma}$ which expresses the stress relative to the current configuration, the 1st Piola-Kirchhoff stress tensor $\boldsymbol{P}$ relates forces in the current configuration with areas in the reference configuration. Similarly, there is another important stress tensor $\boldsymbol{S}$, named the 2nd Piola-Kirchhoff stress tensor, which relates forces in the reference configuration to areas also in the reference configuration. The relationship among them are

$$\boldsymbol{P} = J\boldsymbol{\sigma} \cdot \boldsymbol{F}^{-T} \tag{9}$$

and

$$\boldsymbol{S} = J\boldsymbol{F}^{-1} \cdot \boldsymbol{\sigma} \cdot \boldsymbol{F}^{-T} \tag{10}$$

According to the knowledge in continuum mechanics, the 2nd Piola-Kirchhoff stress tensor $\boldsymbol{S}$ is energy conjugate to the Green-Lagrange strain tensor $\boldsymbol{E}$ and can be obtained by

$$\boldsymbol{S} = \boldsymbol{C} : \boldsymbol{E} \tag{11}$$

where the stiffness tensor, $\boldsymbol{C}$, is a 4th rank tensor and can represent generalized material behavior, isotropic or orthotropic, as long as it is linear, and $\boldsymbol{E}$ can be evaluated in terms of $\boldsymbol{F}$ by

$$\boldsymbol{E} = \frac{1}{2}(\boldsymbol{F}^T \cdot \boldsymbol{F} - \mathbf{I}) \tag{12}$$

In particular, for isotropic materials under Hooke's law, Eq. (11) simplifies to

$$\boldsymbol{S} = \lambda \ \mathrm{tr}(\boldsymbol{E})\, \mathbf{I} + 2\mu \boldsymbol{E} \tag{13}$$

with Lame coefficients λ and μ. Given a material characterized by the Poisson ratio ν^s ($\nu^s < 0.5$ for a compressible structure) and by the Young modulus E^s, bulk modulus K^s, shear modulus G^s and forementioned Lame coefficients λ and μ can be expressed as

$$K^s = \frac{E^s}{3(1-2\nu^s)} \tag{14}$$

$$\mu = G^s = \frac{E^s}{2(1+\nu^s)} \tag{15}$$

$$\lambda = \frac{E^s \nu^s}{(1+\nu^s)(1-2\nu^s)} \tag{16}$$

Substituting Eqs. (10), (13) into (9), we finally calculate the 1st Piola-Kirchhoff stress tensor $\boldsymbol{P}$ in Eq. (8) with

$$\boldsymbol{P} = \boldsymbol{F}\left[\lambda \ \mathrm{tr}(\boldsymbol{E})\, \mathbf{I} + 2\mu \boldsymbol{E}\right] \tag{17}$$

2. Numerical modeling

In this section, we present the modeling in detail. We initialize the simulations with particles on Cartesian lattice using a constant particle spacing Δx. Each particle is assigned a constant mass, which might be different between fluid and structure according to their individual densities. For convenience of explanation, we make some remarks in advance. In the following SPH discretization, the labels a and b are used to denote fluid particles while labels i and j indicating structure particles. An identical kernel function is employed for formulating both fluid and structure equations. Smoothing length h is constant in the entire computational domain.

2.1 *SPH discretization for fluid equations*

(1)Density evolution equation

The density of a fluid particle a is calculated from a summation over all its neighboring particles by

$$\rho_a = m_a \sum_b W_{ab} + m_a \sum_j W_{aj} \tag{18}$$

where ρ_a and m_a denote the density and mass of particle a, W_{ab} is short for kernel function $W(|\boldsymbol{r}_{ab}|, h)$ with $\boldsymbol{r}_{ab} = \boldsymbol{r}_a - \boldsymbol{r}_b$. Note that Eq. (18) allows for density discontinuities across fluid-structure interfaces, and the two terms on the right hand side represent the density contribution from neighboring fluid and structure particles, respectively.

(2) Momentum equation

Including the action due to FSI, the momentum-

conservation Eq. (2) for fluid particle a can be reformed to

$$\frac{\mathrm{d}\boldsymbol{v}_a}{\mathrm{d}t} = \boldsymbol{f}_a^{f:p} + \boldsymbol{f}_a^{f:v} + \boldsymbol{f}_a^{s:p} + \boldsymbol{f}_a^{s:v} + \boldsymbol{g} \tag{19}$$

Here $\boldsymbol{f}_a^{f}$ denotes force per unit mass due to the other fluid particles while $\boldsymbol{f}_a^{s}$ due to structure particles. Both of them consist of two parts, resulting from pressure and viscous force respectively, denoted by $\boldsymbol{f}_a^{f:p}$, $\boldsymbol{f}_a^{f:v}$, $\boldsymbol{f}_a^{s:p}$ and $\boldsymbol{f}_a^{s:v}$.

According to Hu and Adams' work[19], $\boldsymbol{f}_a^{f:p}$ can be approximated by

$$\boldsymbol{f}_a^{f:p} = -\frac{1}{m_a}\sum_b (V_a^2 + V_b^2)\tilde{p}_{ab}\nabla_a W_{ab} \tag{20}$$

where the density-weighted inter-particle averaged pressure $\tilde{p}_{ab}$ is formularized by

$$\tilde{p}_{ab} = \frac{\rho_a p_b + \rho_b p_a}{\rho_a + \rho_b} \tag{21}$$

$\nabla_a W_{ab} = \nabla_a W(\boldsymbol{r}_{ab}, h)$ is the gradient of the kernel function, V_a and V_b denote the two interacting particle volumes.

Using the inter-particle-averaged shear viscosity

$$\tilde{\eta}_{ab} = \frac{2\eta_a\eta_b}{\eta_a + \eta_b} \tag{22}$$

the viscous force $\boldsymbol{f}_a^{f:v}$ can be obtained through

$$\boldsymbol{f}_a^{f:v} = -\frac{1}{m_a}\sum_b \tilde{\eta}_{ab}(V_a^2 + V_b^2)\frac{v_{ab}}{r_{ab}}\frac{\partial W_{ab}}{\partial r_{ab}} \tag{23}$$

with $\boldsymbol{v}_{ab} = \boldsymbol{v}_a - \boldsymbol{v}_b$ and $r_{ab} = |\boldsymbol{r}_{ab}|$ representing the relative velocity and distance between two interacting particles.

Based on the analysis of Turek et al.[20], the boundary condition on the fluid-structure interface can be achieved by exerting a no-slip condition for the flow with moving boundaries. Following the implementation of Adami et al.'s wall boundary condition[21] and assuming the dummy particles in structure region used to mimic the interaction on the fluid-structure interface just coincide with the real structure particles, for each interacting particle pair (a, i), we can simply approximate the imagining pressure p_i^d and velocity $\boldsymbol{v}_i^d$ on dummy particle i with

$$p_i^d = p_a \tag{24}$$

and

$$\boldsymbol{v}_i^d = 2\boldsymbol{v}_i - \boldsymbol{v}_a \tag{25}$$

Alternatively, one can also choose the same extrapolation scheme proposed in Ref. [21] to evaluate them.

Consequently, the forces per unit mass due to structure particles $\boldsymbol{f}_a^{s:p}$ and $\boldsymbol{f}_a^{s:v}$ can be given by

$$\boldsymbol{f}_a^{s:p} = -\frac{1}{m_a}\sum_j (V_a^2 + V_j^2)p_a\nabla_a W_{aj} \tag{26}$$

and

$$\boldsymbol{f}_a^{s:v} = \frac{1}{m_a}\sum_j \eta_a(V_a^2 + V_j^2)\frac{\boldsymbol{v}_a - \boldsymbol{v}_j^d}{r_{aj}}\frac{\partial W_{aj}}{\partial r_{aj}} = \frac{2}{m_a}\sum_j \eta_a(V_a^2 + V_j^2)\frac{\boldsymbol{v}_a - \boldsymbol{v}_j}{r_{aj}}\frac{\partial W_{aj}}{\partial r_{aj}} \tag{27}$$

Since the negative pressure occurs in the wake in the FSI benchmark cases, which usually leads to particle clumping and void regions during the simulation, one also needs a remedy to solve this tensile instability problem in fluid regions. A number of solutions have already been proposed and validated, such as in Refs. [16, 17]. In this work, we choose transport-velocity scheme exactly the same as that in Ref. [17] (see details therein).

2.2 *SPH dicretization for structure equations*

Before formulating the momentum balance Eq. (8) for structure with SPH approximation, we must make some preparations first. It is well known that the conventional SPH method has a shortcoming of inconsistency, not even zero order consistency[22]. It may not be that important in fluid dynamics, however, it leads to artificial strain and stress in solid dynamics, especially when a rigid coordinate transformation occurs on a structure, where no actual strain and stress should be yielded. To remedy this defect, a correction matrix $\boldsymbol{B}^0$, following Vignjevic et al.[15], is introduced by

$$\boldsymbol{B}_i^0 = \left[\sum_j V_j^0(\boldsymbol{X}_j - \boldsymbol{X}_i)\otimes\nabla_i^0 W_{ij}\right]^{-1} \tag{28}$$

where

$$\nabla_i^0 W_{ij} = \frac{\partial W\left(\left|\boldsymbol{r}_{ij}^0\right|, h\right)}{\partial r_{ij}^0} \boldsymbol{e}_{ij}^0 \tag{29}$$

is the gradient of a Lagrangian kernel function. Note that Eqs. (28) and (29) are only calculated once at the beginning as it is only related to the initial or reference configuration.

Multiplying by the same matrix $\boldsymbol{B}^0$, the deformation gradient $\boldsymbol{F}$ can be computed with SPH approximation by

$$\boldsymbol{F}_i = \left[\sum_j V_j^0 (\boldsymbol{u}_j - \boldsymbol{u}_i) \otimes \nabla_i^0 W_{ij}\right] \boldsymbol{B}_i^0 + \mathbf{I} \tag{30}$$

(1) Density evolution equation:

According to Eq. (7), the density of each structure particle i can be obtained algebraicly by

$$\rho_i = \frac{1}{J_i} \rho_i^0 \tag{31}$$

with $J_i = \det(\boldsymbol{F}_i)$.

(2) Momentum balance equation:

Similar as that in fluids, when including the action due to FSI, the momentum balanceEq. (8) for structure particle i should be reformed with additional terms to

$$\frac{\mathrm{d}^2 \boldsymbol{x}_i}{\mathrm{d}t^2} = \boldsymbol{f}_i^{s:P} + \boldsymbol{f}_i^{f:p} + \boldsymbol{f}_i^{f:v} + \boldsymbol{g} \tag{32}$$

where $\boldsymbol{f}_i^{s:P}$ denotes the acceleration caused by inner stress of a structure. It can be represented by

$$\boldsymbol{f}_i^{s:P} = \frac{1}{m_i} \sum_j \left[(V_i^0)^2 + (V_j^0)^2\right] \frac{\boldsymbol{P}_i \boldsymbol{B}_i^0 + \boldsymbol{P}_j \boldsymbol{B}_j^0}{2} \cdot \nabla_i^0 W_{ij} \tag{33}$$

with the 1st Piola-Kirchhoff stress tensor of particle i being

$$\boldsymbol{P}_i = \boldsymbol{F}_i \left[\lambda \operatorname{tr}(\boldsymbol{E}_i)\, \mathbf{I} + 2\mu \boldsymbol{E}_i\right] \tag{34}$$

and Green-Lagrange strain tensor

$$\boldsymbol{E}_i = \frac{1}{2}(\boldsymbol{F}_i^{\mathrm{T}} \cdot \boldsymbol{F}_i - \mathbf{I}) \tag{35}$$

Finally, according to the Newton's third law of motion, each structure particle involved in Eqs. (26) and (27) takes an equal and opposite reaction from the interacting fluid particle, therefore, the forces per unit mass owing to fluid-structure interactions can be given easily by

$$\boldsymbol{f}_i^{f:p} = -\frac{1}{m_i} \sum_b (V_i^2 + V_b^2) p_b \nabla_i W_{ib} \tag{36}$$

and

$$\boldsymbol{f}_i^{f:v} = \frac{2}{m_i} \sum_b \eta_b (V_i^2 + V_b^2) \frac{\boldsymbol{v}_i - \boldsymbol{v}_b}{r_{ib}} \frac{\partial W_{ib}}{\partial r_{ib}} \tag{37}$$

Notice that, the gradient of elastic stress in structures is calculated in the reference configuration within the total Lagrangian formulation, however, the fluid-structure interaction forces must be obtained in the current configuration.

3. Numerical test

In this section, we present the validation results for the well-known 2-D benchmark FSI problem, defined by Turek and Hron[20], as shown in the Fig. 1, where the flow passes a fixed circular cylinder with a flexible beam attached to its downstream side. This test model has been frequently used as a large-displacement benchmark validation case for 2-D FSI solvers[5, 23].

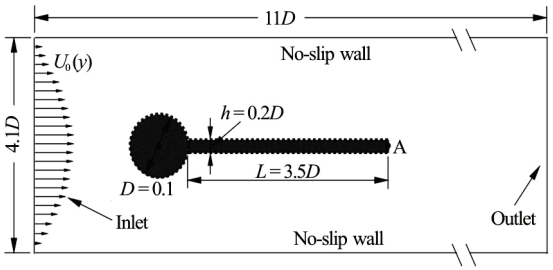

Fig. 1 Model setup for flow-induced vibration of a flexible beam attached to a rigid cylinder[5]

In Fig.1, the computational domain is sketched out along with all its geometric parameters. By choosing the cylinder diameter $D = 0.1$ m as the characteristic length, all other spatial measurements can be represented by D, such as the domain length $L = 11D$, the domain height $H = 4.1D$, and the length and height of the flexible beam being $l = 3.5D$ and $h = 0.2D$, respectively. Note that, the cylinder center is located at $C = (0.2D, 0.2D)$ (measured from the left bottom corner of the domain), which is intentionally non-symmetric to prevent the dependence of the onset of any possible oscillation on the precision of the computation[20].

Concerning boundary conditions, no-slip walls are exerted on the top and bottom sides of the domain while outflow condition on the right side. Fluid flows into the domain from the left side with a parabolic velocity profile

$$U_0(y)=1.5\overline{U}\frac{y(H-y)}{\left(\frac{H}{2}\right)^2} \tag{38}$$

where $\overline{U}$ is the mean inflow velocity with the value of 1m/s in this paper. As suggested by Turek and Hron[20], for this kind of non-steady test case, a starting procedure is usually applied by employing a smooth increase of the velocity profile in time as:

$$U(t,y)=\frac{1-\cos\left(\frac{\pi t}{2}\right)}{2}U_0(y) \quad \text{if} \quad t<T_s \tag{39a}$$

$$U(t,y)=U_0(y) \quad \text{otherwise} \tag{39b}$$

where T_s denotes the end time of the starting procedure.

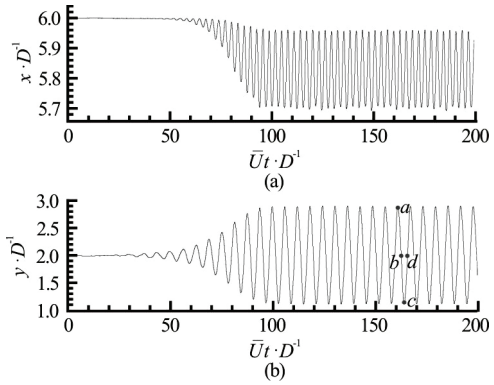

Fig. 2 Temporal variation of x and y displacements of the Point A

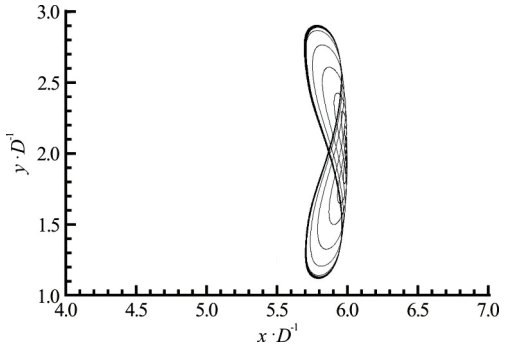

Fig. 3 Trajectory of Point A

With the same configuration shown above, Turek and Hron[20] defined three different test cases FSI1, FSI2 and FSI3 by considering different physical parameters corresponding to Reynolds number $Re=20$, $Re=100$ and $Re=200$, respectively. FSI1 is "simple" and results in a steady state solution while the other two tests (FSI2, FSI3) result in periodic solutions. Because the shear modulus of the beam in FSI3 is four times larger than that in FSI2, the fluid structure interaction in FSI3 seems more like fluid interacting with rigid body. In contrast, FSI2 consists of a more flexible beam and is considered more suitable and challenging as the benchmark test case for the rigorous evaluation of different FSI approaches. Therefore, we just focus on the test of FSI2 in this work. Here, the dimensionless parameters are chosen as follows: density ratio of structure to fluid $\rho_s/\rho_f=10$, Reynolds number $Re=\rho_f\overline{U}D/\eta=100$, dimensionless Young's modulus $E^*=E/(\rho_f\overline{U}^2)=1.4\times10^3$ and Poisson ratio $\nu^s=0.4$. In the simulation, the initial particle spacing is set to be $\Delta x=0.05D$, the artificial sound speed $c_0=20\overline{U}$, and a Wendland C2[24] kernel function with a pre-set smoothing length $h=1.3\times\Delta x$ is used.

The time evolution of the x and y displacements of the free end of the beam (calculated at point A as marked in Fig. 1) is shown in Fig. 2. According to the y displacement, we can see the beam begins to exhibit small deformations after a dimensionless time of around 20, at which the starting procedure finishes in the simulation. As time goes on, the beam finally reaches a periodic self-sustained oscillation after a dimensionless time of 100. At this moment, an offset along the negative x direction can be clearly observed due to the effect of the beam's bending. Figure 3 presents the trajectory of point A during the simulation, which is a typical Lissajous curve with the frequency ratio of horizontal wave to vertical wave being 2:1.

Table 1 Comparison results for FSI2 test case

Reference	Amplitude in y direction $(/D)$	Frequency f_0
Turek and Hron[20]	0.830	0.190
Bhardwaj and Mittal[23]	0.920	0.190
Tian et al.[5]	0.784	0.190
Present	0.886	0.168

Table 1 shows the quantitative comparison of the present results with those in references. The dimensionless amplitude of the oscillation in y direction from our simulation is 0.886, which is in good agreement with others. However, the dimensionless oscilla-

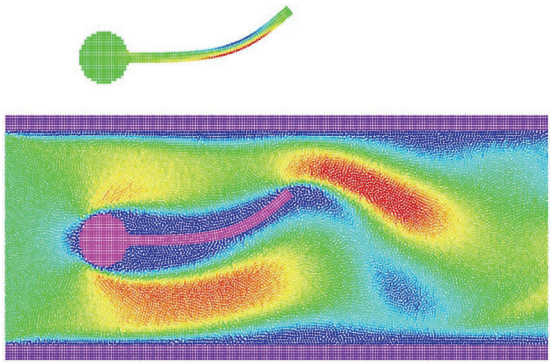

(a) Time instance a

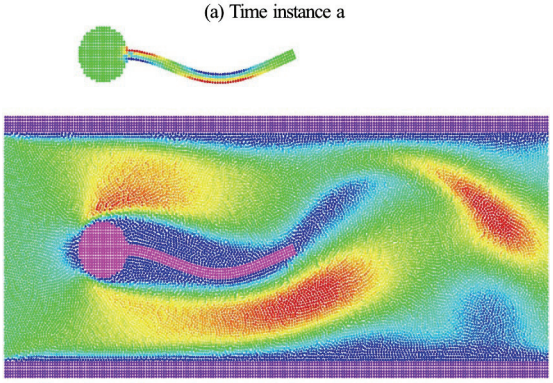

(b) Time instance b

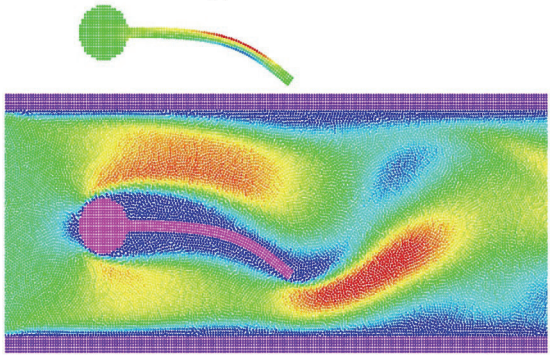

(c) Time instance c

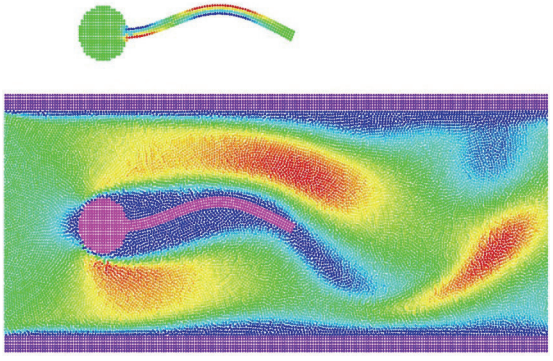

(d) Time instance d

Fig. 4 (Color online) The fluid velocity field and beam deformation at different time instances marked in Fig. 2. The top panel of each subfigure shows the deformation of the beam with solid particles colored by contours of von Mises stress. The bottom panel presents the distribution of axial velocity component of the fluid

tion frequency obtained in this work cannot match well with them. To further validate the present frequency, we perform a convergence study on this test case by decreasing the particle spacing Δx to $0.025D$. Almost the same frequency is obtained. To analyze the apparent discrepancy with previous results, we resort to investigate the phenomenon of vortex shedding[25] behind circular cylinders. Based on Roshko's measurements[26], there is a fairly consistent unique linear relationship between the Roshko number and Reynolds number over the Reynolds number range 50-150, which can be formulated by

$$Ro = 0.212Re - 4.5 \tag{40}$$

where Ro denotes Roshko number. According to Eq. (40), we know that the frequency of vortex shedding at $Re = 100$ is 0.167. Since the beam is very flexible in this test case, the oscillation frequency can be mainly dominated by vortex shedding, which means the oscillation frequency of the beam might also be close to this number. Besides, because our scheme is strictly momentum-conservative in contrast to those in the references, it is expected that the present result can be quite reasonable.

In Fig.4 we show the beam deformation at four different time instances in a typical oscillation cycle. Note that, since there is no elastic stress at the free end of the beam, particles in that region keep regular distribution all the time. This is not able to achieve by the previous SPH formulations based the incremental Jaumann formulation which uses Eulerian kernel in current configuration.

4. Conclusion

In this paper, we have proposed a numerical modeling approach for simulating FSI problems in a SPH framework, where the fluid governing equations are discretized with conventional Eulerian kernel in current configuration and the solid governing equations with Lagrangian kernel in the reference configuration. To avoid tensile instability in fluid regions, a transport-velocity technique is employed to remedy the distribution of fluid particle. By using a total Lagrangian SPH formulation dealing with the structure deformations, we also apply a correction matrix to restore first order consistency and rotational invariance. It successfully avoids the occurrence of artificial strain and stress when a rigid coordinate transformation occurs on structures. Since both fluid and solid governing equations are discretized with SPH formulation, coupling becomes straightforward and meanwhile the momentum of an FSI system is strictly conserved. In order to validate the modeling and demonstrate its potential, a typical FSI benchmark

test case is carried out.

Acknowledgement

The authors gratefully acknowledge the financial support by Deutsche Forschungsgemeinschaft (Grant No. DFG HU1527/6-1) for the present work.

References

[1] Bungartz H. J., Schäfer M. Fluid-structure interaction. Modelling, simulation, optimisation [M]. Berlin, Heidelberg, Germany: Springer Science and Business Media, 2006.

[2] Sigrist J. F. Fluid-structure interaction: An introduction to finite element coupling [J]. *Comptuters and Mathematics with Applications*, 2015, 69(10): 1167-1188.

[3] Tezduyar T. E., Sathe S., Keedy R. Space–time finite element techniques for computation of fluid–structure interactions [J]. *Computer methods in Applied Mechanics and Engineering*, 2006,195(17): 2002-2027.

[4] Ahn H. T., Kallinderis Y. Strongly coupled flow/structure interactions with a geometrically conservative ALE scheme on general hybrid meshes [J]. *Journal of Computational Physics*, 2006, 219(2): 671-696.

[5] TianF. B., DaiH., Luo H. Fluid–structure interaction involving large deformations: 3D simulations and applications to biological systems [J]. *Journal of computational physics*, 2014, 258(2): 451-469.

[6] Wu K., Yang D., Wright N. A coupled SPH-DEM model for fluid-structure interaction problems with free-surface flow and structural failure [J]. *Computers and Structures*, 2016, 177: 141-161.

[7] Han K., Feng Y.T., Owen D.R. J. Numerical simulations of irregular particle transport in turbulent flows using coupled LBM-DEM [J]. *Computer Modeling in Engineering and Sciences*, 2007, 18(2):87-100.

[8] Liu G. R., Liu M. B. Smoothed particle hydrodynamics: A meshfree particle method [M]. Singopare: World Scientific, 2003.

[9] Lucy L. B. A numerical approach to the testing of the fission hypothesis [J]. *Astronomical Journal*, 1977, 82: 1013-1024.

[10] Gingold R. A., Monaghan J. J. Smoothed particle hydrodynamics: Theory and application to non-spherical stars [J]. *Monthly Notices of the Royal Astronomical Society*, 1977, 181(3): 375-389.

[11] Antoci C., Gallati M., Sibilla S. Numerical simulation of fluid–structure interaction by SPH [J]. *Computers and Structures*, 2007, 85(11-14): 879-890.

[12] Gray J. P., Monaghan J. J., Swift R. P. SPH elastic dynamics [J]. *Computer Methods in Applied Mechanics and Engineering*, 2001, 190(49): 6641-6662.

[13] Zhang C., Hu Y., Adams N. A. A generalized transport-velocity formulation for smoothed particle hydrodynamics [J]. *Journal of Computational Physics*, 2017, 337: 216-232.

[14] Libersky L. D., Petschek A. G., Carney T. C. et al. High strain Lagrangian hydrodynamics: A three-dimensional SPH code for dynamic material response [J]. *Journal of computational physics*, 1993, 109(1): 67-75.

[15] Vignjevic R., Reveles J. R., Campbell J. SPH in a total Lagrangian formalism [J]. *Computer Modeling in Engineering and Sciences*, 2006, 14(3): 181-198.

[16] Monaghan J. J. SPH without a tensile instability [J]. *Journal of Computational Physics*, 2000, 159(2): 290-311.

[17] Adami S., Hu X. Y., Adams N. A. A transport-velocity formulation for smoothed particle hydrodynamics [J]. *Journal of Computational Physics*, 2013, 241(5): 292-307.

[18] Monaghan J. J. Simulating free surface flows with SPH [J]. *Journal of computational physics*, 1994, 110(2): 399-406.

[19] Hu X. Y., Adams N. A. A multi-phase SPH method for macroscopic and mesoscopic flows [J]. *Journal of Computational Physics*, 2006, 213(2): 844-861.

[20] Turek S., Hron J. Proposal for numerical benchmarking of fluid-structure interaction between an elastic object and laminar incompressible flow (Bungartz H. J., Schäfer M. Fluid-structure interaction: Modeling, simulation, optimisation) [M]. Berlin, Heidelberg, Germany: Springer, 2006, 371-385.

[21] Adami S., Hu X. Y., Adams N. A. A generalized wall boundary condition for smoothed particle hydrodynamics [J]. *Journal of Computational Physics*, 2012, 231(21): 7057-7075.

[22] Bonet J., Kulasegaram S. A simplified approach to enhance the performance of smooth particle hydrodynamics methods [J]. *Applied Mathematics and Computation*, 2002, 126(2): 133-155.

[23] Bhardwaj R., Mittal R. Benchmarking a coupled immersed-boundary-finite-element solver for large-scale flow-induced deformation [J].*AIAA Journal*, 2012, 50(7): 1638-1642.

[24] Wendland H. Piecewise polynomial, positive definite and compactly supported radial functions of minimal degree [J]. *Advances in computational Mathematics*, 1995, 4(1): 389-396.

[25] Gaster M. Vortex shedding from circular cylinders at low Reynolds numbers [J]. *Journal of Fluid Mechanics*, 1971, 46: 749-756.

[26] Roshko A. On the development of turbulent wakes from vortex streets [R]. Technical Report Archive and Image Library, 1954.